1 **Testing ground based observations of wave activity in the (lower and upper) atmosphere**
2 **as possible (complementary) indicators of streamer events**

3 **Michal Kozubek[1], Lisa Kuchelbacher[2], Jaroslav Chum[1], Tereza Sindelarova[1], Franziska**
4 **Trinkl[2, a], Katerina Podolska[1]**

5 [1]Institute of Atmospheric Physics CAS, Bocni II 1401, Prague, 14100, Czech Republic

6 [2] Earth Observation Center, Deutsches Zentrum für Luft- und Raumfahrt,82234 Weßling,
7 Germany
8 [a] now at Karlsruhe Institute of Technology (KIT), Institute of Meteorology and Climate
9 Research, Karlsruhe, Germany

10 **Correspondence: Michal Kozubek, kom@ufa.cas.cz**

12

13 **Abstract:** For a better understanding of atmospheric dynamics, it is very important to know
14 the general condition (dynamics and chemistry) of the atmosphere. Planetary waves (PWs) are
15 global scale waves, which are well-known as main drivers of the large-scale weather patterns
16 in mid-latitudes on time scales from several days up to weeks in the troposphere. When PWs
17 break, they often cut pressure cells off the jet stream. A specific example are so-called
18 streamer events, which occur predominantly in the lower stratosphere at mid- and high-
19 latitudes. For streamer events we check, whether there are any changes of gravity wave (GW)
20 or infrasound characteristics related to these events in ionospheric and surface measurements
21 (continuous Doppler soundings, two arrays of microbarometers) in the Czech Republic.

22 Phenomena in infrasound arrival parameters undoubtedly related with streamer events were
23 not identified in observations of two stations located in Central Europe. Simulations of
24 infrasound propagation show influences of the streamer events on the waveguide formed near
25 the tropopause. Microbarom propagation is influenced by the tropopause waveguide in a
26 limited azimuth sector and at limited distances. Due to the typical occurrence of the streamer
27 events over the North Atlantic, infrasound stations in Western Europe can be of particular
28 interest for future studies of streamer event signatures in infrasound arrivals. Arrivals to
29 Central Europe are through the waveguide formed between the ground and the upper
30 stratosphere. The upper stratosphere waveguide is not influenced by the streamer events.

Supplementary ground-based measurements of GW using the WBCI array in the troposphere showed that GW propagation azimuths were more random during streamer and streamer-like events compared to those observed during calm conditions. GW propagation characteristics observed in the ionosphere by continuous Doppler soundings during streamer events did not differ from those expected for the given time period.

1) Introduction

For a better comprehension of climate change it is fundamentally important, how well we understand the climate system in general, and the dynamics of the atmosphere in particular. The dynamical processes relevant in this context in the atmosphere take place over a comparatively wide range of scales in space and time. They include in particular both, planetary and gravity waves. Planetary waves are the main drivers of the extratropical circulation. When they break, they lead to an irreversible exchange of air masses between the equatorial and polar region due to an amplification of their amplitudes (e.g. McIntyre & Palmer, 1983; Polvani & Plumb,1992). In the lower stratosphere ozone can be used as a tracer for these large-scale motions, as it has a comparatively long life-time. When planetary waves break tropical air masses of low ozone concentration are mixed poleward into the sourrounding atmosphere of the mid and higher latitudes (e.g. Leovy et al., 1985).

The term "streamer" lacks a precise definition, as noted by Krüger et al. (2005). They discuss various aspects of streamers, including their impact on mixing and the divergent definitions associated with them. Offermann et al. (1999) describe streamers as large-scale tongue-like structures formed by the meridional deflection of air masses. Streamers are characterized by irreversible mixing of air masses between equatorial and polar regions which is why they might be linked to planetary wave breaking (Waugh, 1993). Eyring et al. (2003) give a climatology of the seasonal and geographical distribution of streamer events. They show, that streamers often occur over the Northern Atlantic and can be identified by either high NO_2 or low ozone concentration, which is why we select streamers by total ozone column measurements. They show that streamer events occur most often during winter and least during July and August in the Northern Hemisphere. During a streamer event the wind field changes rather strong over a comparatively small distance. Since a streamer event shows a strong wind shear at its flanks, it is expected that it excites GW (e.g. Kramer et al., 2015 and 2016 or Peters et al., 2003).

It is well-known that enhanced wind gradients or anticyclones can lead to the excitation of gravity waves (GW) in the atmosphere (e.g. Pramitha et al., 2015; Kai et al., 2010; Kramer et al., 2015, 2016 and Gerlach et al., 2003). GW have typical vertical wavelengths from a few 100 m to several kilometres (Wüst & Bittner, 2006), and horizontal wavelenghts over tens of km (Wüst et al., 2018), and longer (Rauthe et al., 2006); their fluctuations in the upper troposphere / lower stratosphere typically show amplitudes of 5–10 m/s at maximum (e.g., Kramer et al., 2015). Those waves transport energy and momentum horizontally and vertically through the atmosphere and deposit them especially in the stratosphere and mesosphere but also above and below this height region. The propagation of GWs is strongly dependent on the wind conditions in the stratosphere since the wind speed of the middle atmosphere (10–100 km) reaches its maximum there. That is why monitoring waves in upper parts of the atmosphere, e.g. based on Doppler observations in the ionosphere, can provide additional information about stratospheric conditions (for details see Fritts and Alexander, 2003).

Using pressure recordings at a microbarograph array, GWs and infrasound at the ground can be observed. Ground based observations of GWs at a large aperture microbarograph array are utilized in the present study as an independent data source for the analysis of GW activity during streamer events. Infrasound propagation is influenced by wind and temperature fields in the atmosphere. Three regions play an important role in long-distance infrasound propagation: (1) the lower thermosphere; (2) the stratosphere; (3) the jet stream near the tropopause and inversion layers in the troposphere (Evers and Haak, 2010). Infrasound observed at the ground and emitted by distant sources mostly propagates in the stratospheric waveguide (Ceranna et al., 2019). The thermospheric waveguide is not as efficient as the stratospheric waveguide in the long-range infrasound propagation. Besides signal loss due to geometrical spreading, infrasound absorption is important in the upper atmosphere (Bittner et al., 2010). Infrasound absorption is proportional to the frequency; higher frequencies, particularly those above 1 Hz undergo stronger absorption in the thermosphere (Sutherland and Bass, 2004). Signal attenuation is low at frequencies of the order of $10^{-3} - 10^{-2}$ Hz (Blanc, 1985; Georges, 1968).

A number of case studies have proved that stratospheric dynamics can be deduced from microbarograph measurements at the ground (Assink et al., 2014; Blixt et al., 2019; Evers and Siegmund, 2009; Evers et al., 2012; Garcès et al., 2004; Le Pichon and Blanc, 2005; Le Pichon et al., 2006 and 2009; Smets and Evers, 2014). Streamer events are significant

96   transient disturbances to circulation patterns in the tropopause/lower stratosphere region;

97   modifications of the stratospheric waveguide can therefore be expected. A feasibility study on

98   utilisation of ground infrasound measurements in research of streamer events is performed. Its

99   aim is to identify phenomena in infrasound detections related to the streamers; we focus on

100   deviations of the azimuth of signal arrivals, trace velocity, signal amplitude, and frequency.

101   The dedicated studies demonstrated that from the observed signal trace velocity, information

102   about the signal refraction height can be derived (Lonzaga, 2015). If the source of received

103   signals is well defined in time and space, mean atmospheric cross-winds along the signal

104   propagation path can be estimated from back-azimuth deviations and time of signal

105   propagation (Blixt et al., 2019). Fluctuations of signal frequency and amplitude are, besides

106   variability of the signal source influenced by atmospheric filtering (Sutherland and Bass,

107   2004).

108   Our study will focus on possible utilization Doppler sounding and microbarographs for

109   description and analysis of GW behaviour and propagation in the stratosphere.

110   The structure of the paper is as follows: After introduction the description of the used dataset

111   and method can be found in the second section. Then we describe our results and in the last

112   section we discuss the possible connection to previous studies.

113

2) Data and methods

115   The selection of streamer events is based on the visual inspection of global maps of total

116   ozone column (TO3), accessible through a service provided by DLR

117   (https://atmos.eoc.dlr.de/) measured by the Tropospheric Monitoring Instrument (TROPOMI)

118   aboard the Sentinel 5 Precursor (S5P) mission. See Veefkind et al., 2012 for details about

119   TROPOMI/S5P. In cases where TROPOMI/S5P data is unavailable, measurements from the

120   Global Ozone Monitoring Experiment-2 (GOME-2) on the Metop series of satellites are

121   utilized. Both instruments operate in a nadir-viewing configuration on near-polar sun-

122   synchronous orbits. Further specifics regarding TO3 measurements by TROPOMI/S5P are

123   elaborated by Spurr et al. (2022). The TO3 retrieval process is built upon the predecessor

124   instrument's processor, with GOME-2 on Metop-AB, see Munro et al. (2006) and Munro et al.

(2016). For detailed information on the GOME-2 retrieval algorithm, refer to Loyola et al. (2011).

We define a streamer as such when the ozone column concentration of the finger-like structure above the Northern Atlantic/Western Europe is lower than 300 DU and persists for at least 3 days. The longitudinal extension is of approx. 15 to 30 degrees in the mid-latitudes (between 30 to 70°N). The northernmost point of a streamer exceeds 50°N. Fig. 1 shows a streamer event above the Northern Atlantic, indicated by the blue color which represent the low ozone concentrations. The streamer shown in Ffig. 1 reaches latitudes beyond 70°N, which indicates a large example. At the western and eastern flanks of the streamer, the ozone concentration exceeds 350 DU, defining distinct boundaries. This is also visible in fFig. 1 represented by the green colors at the eastern coast of Northern America and western Europe. So, there is a gradient of the ozone concentration of about 50 DU / 5°. Furthermore, the streamer exhibits a discernible pattern of circulation, with air masses being meridionally deflected, contributing to its formation and maintenance. These air masses, characterized by their movement from south to north at the eastern flank and from north to south at the western flank, play a significant role in the streamer's dynamics. This is the reason why equatorial low ozone concentration is transported northward. In contrast, the calm periods, representing the opposite dynamic situation to the streamer events, are characterized by only very few meridionally deflected air masses. During these periods, the ozone concentration in the mid-latitudes above the Northern Atlantic is consistently higher than 350 DU, indicating stable atmospheric conditions and minimal perturbations in the ozone distribution. An example for a calm period is shown in Fig. 2.

The streamer events are selected by eye for this study (results see Table 1) considering the TO3 global maps from January 2020 and March 2021. As planetary waves are permanently disturbing the atmospheric dynamic of the higher troposphere / lower stratosphere, especially smaller scale streamers can be observed almost every day and the identification of streamer events becomes subjective. We therefore focus on few events which are comparatively strong in their evolution from our perspective. Moreover, we focus on streamer events above the Northern Atlantic. Whenever another streamer event occurs somewhere other than over the Northern Atlantic region with comparable spatiotemporal extent, we do not consider this date as a streamer event. We assume that the effects of the streamer superimpose and a distinct backtrack to the streamer over the Northern Atlantic will not be possible. This means, that the analysis of the streamer events can be blurred to some extent.

158 We consider dates from January 2020 to April 2021. In general, planetary waves drive the
159 Brewer Dobson Circulation in the stratosphere during winter and ozone-poor airmasses are
160 transported northward. Streamer events are therefore detected between September and March.
161 The streamer events are distinguished if they have a large spatial size, high intensity (low
162 TO3 concentration) and if air masses are irreversibly mixed into the surrounding atmosphere.
163 All the selected events persist for several days, but no longer than 10 days.

164 To evaluate whether streamer events effect the smaller-scale atmospheric dynamics, calm
165 events are identified as well by subjective criteria. These events serve as a reference to
166 streamer events, as large-scale spatial structures are hardly visible in the TO3. The events are
167 selected when the ozone concentration shows a meridional gradient from the equator to polar
168 region on the Northern Hemisphere with almost no longitudinal variation. The examples of
169 calm atmospheric dynamics are listed in Table 1 (right).

170

Streamer events		Calm periods	
From	**To**	**From**	**To**
06.02.2020	10.02.2020	02.03.2020	08.03.2020
11.2.2020	13.2.2020	09.03.2020	14.03.2020
31.08.2020	03.09.2020	28.03.2020	10.04.2020
05.09.2020	11.09.2020	19.04.2020	27.05.2020
03.11.2020	07.11.2020	9.11.2020	15.11.2020
21.11.2020	25.11.2020	12.12.2020	22.12.2020
23.02.2021	27.02.2021	30.12.2020	06.01.2021
09.03.2021	12.03.2021	21.01.2021	20.02.2021
		28.02.2021	07.03.2021
		13.03.2021	24.03.2021
		29.03.2021	07.04.2021

Table 1 Streamer events above Northern Atlantic from January 2020 until March 2021 and related start and end dates. The right part shows calm periods.

Figure 1 shows the TO3 by TOPOMI/S5P integrated from November 3rd to November 5th 2020. Ozone-poor airmasses (blue) are located above the Northern Atlantic from 30°N to 70°N next to smaller scale ozone-poor airmasses above western North America and Central Asia. The TO3 concentration is disturbed by planetary waves along the latitudes, which lead to wave structures visible especially at the transition of blue to green colors. A large streamer event of ozone-poor airmasses is detected over the Northern Atlantic. A small streamer can be detected over western North America. There are also ozone-poor air masses above eastern Europe. The temporal evolution shows, that the ozone-poor air masses above eastern Europe are due to a decaying streamer which evolved several days earlier. As planetary waves are more or less permanently disturbing the atmospheric dynamics, especially smaller scale streamers can be detected almost every day. In this example, the streamer event above the Northern Atlantic is largest. Therefore, we consider this event for the further analysis.
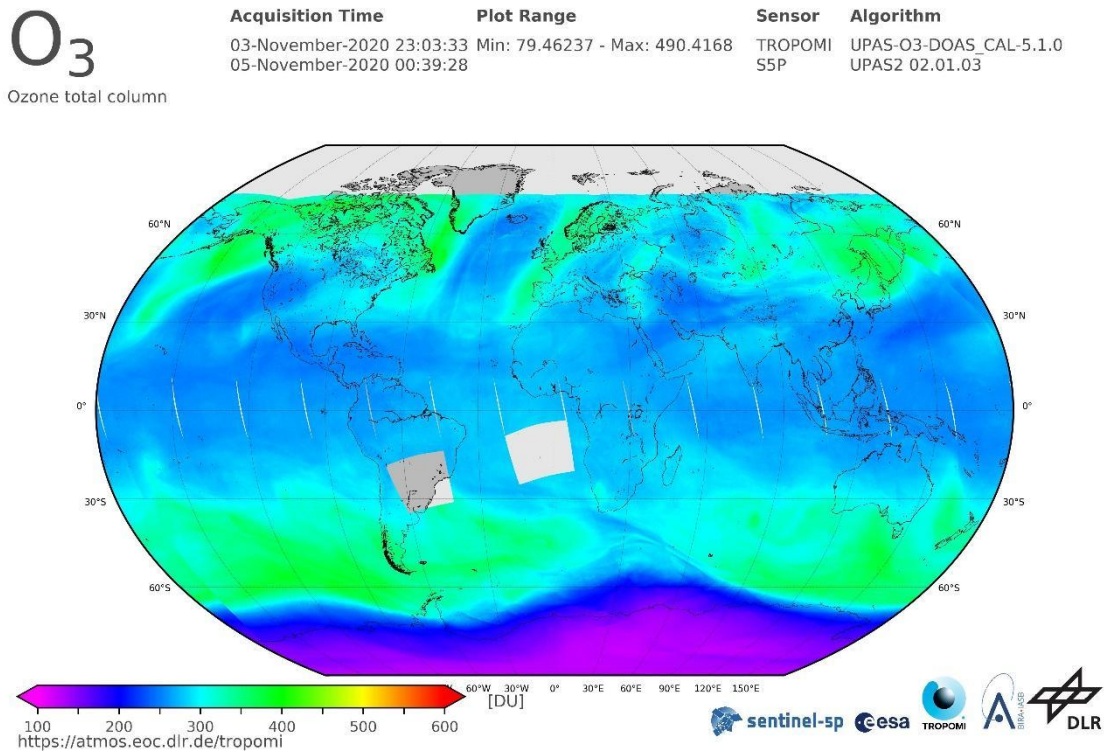
187 Fig. 1. TO3 by TROPOMI/S5P from November 3rd to November 5th 2020 shows ozone poor
188 airmasses above the Northern Atlantic as an example of a streamer event for the further
189 analysis. Colors (from violet to red) indicate the total ozone column concentrations (from low
190 to high) in Dobson Units. Source: DLR, CC-BY 3.0

191

192   Figure 2 shows the TO3 by TOPOMI/S5P from February 11th to February 13th 2020. The

193 event is characterized by a strong meridional gradient from the equatorial to polar region on

194 the Northern Hemisphere with almost no longitudinal variation. Therefore, we consider this

195 event for the further analysis.

196

197 https://atmos.eoc.dlr.de/tropomi
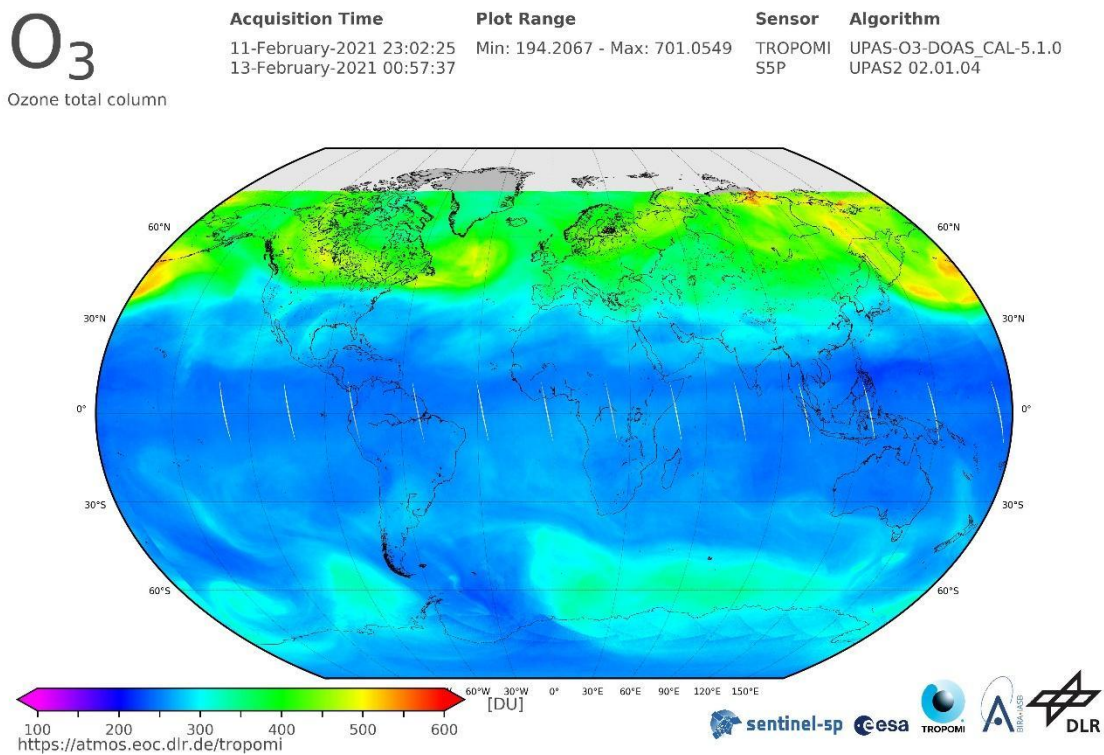
198 Fig. 2. TO3 by TROPOMI/S5P from February 11th to February 13th 2020 as an example of
199 calm atmospheric dynamics. A clear meridional gradient of ozone can be observed on the
200 Northern Hemisphere without large-scale wave structures. Colors (from violet to red) indicate
201 the total ozone column concentrations (from low to high) in Dobson Units. Source: DLR, CC-
202 BY 3.0

203 Two stations of the Czech microbarograph network (Bondar et al., 2022) are involved in the

204 study – the large aperture array WBCI (50.25°N 12.44°E) and the small aperture array PVCI

205 (50.52°N 14.57°E). To study propagation of GW and long-period infrasound (from acoustic

206 cut-off up to about 2.5 s) pressure recordings at WBCI are utilized. Four sensors of the WBCI

207 array are arranged in a tetragon. The inter-element distances of 4 – 10 km define an optimum

208 performance of the array in the infrasound frequency range from the acoustic cut-off

209 frequency of 0.0033 to 0.0068 Hz (Garcès, 2013). The WBCI array with its large inter-

210 element distances has a unique configuration compared to the arrays of the International

211 Monitoring System of the Comperehensive Nuclear Test Ban Treaty Organisation intended

212 for infrasound monitoring in the frequency band of 0.02 – 4 Hz (Marty, 2019). Each array

213 element at WBCI is equipped with an absolute microbarometer of the type Paroscientific

214 6000-16B-IS with parts-per-billion resolution. A GPS receiver is used for time stamping. Data

215 are stored with a sampling rate of 50 Hz. For infrasound monitoring, WBCI data are

216 resampled at 10 Hz sampling rate. To detect and analyze GW, 1-min mean values of the

217 absolute pressure data are used.

218 The small aperture array PVCI provides optimal precision of detections in the frequency

219 range of 0.14 – 3.4 Hz (Garcès, 2013). Three sensors are arranged in an equilateral triangle;

220 the array aperture is 200 m. The differential sensors of the type Infrasound Gage ISGM03

221 manufactured by the Scientific and Technical Centre give a flat response in the frequency

222 range of 0.02 – 4 Hz. A GPS receiver is used for time stamping. The data are stored with a

223 sampling frequency of 25 Hz. This sampling rate is also used in regular processing of

224 infrasound detections at PVCI.

225 Infrasound detections are processed using the DTK-GPMCC software the core of which is the

226 Progressive Multi-Channel Correlation (PMCC) detection algorithm (Cansi, 1995; Le Pichon

227 and Cansi, 2003). PMCC analyses pressure recordings from an infrasound array and looks for

228 coherent signals in overlapping time windows in several frequency bands (Le Pichon and

229 Cansi, 2003). An elementary detection with the PMCC, or the detection pixel is declared in

230 the time-frequency window, when signal correlation and consistency criteria are met.

231 Detection pixels are grouped into the detection families based on similar time, frequency,

232 azimuth of signal arrival, and signal trace velocity (Brachet et al., 2010). The arrival

233 parameters of the detected infrasound are stored in the detection bulletins. The parameters of

234 interest for the present study include time of arrival, azimuth of arrival, trace velocity,

235 frequency, and amplitude. The PMCC configuration is set on an individual basis and is

236 optimized for the given array (Brachet et al., 2010; Garcès, 2013; Szuberla et al., 2004); main

237 parameters of the DTK-GPMCC settings for the arrays PVCI and WBCI are given in Table 2.

Station	PVCI	WBCI
Detection range	0.09-7 Hz	0.0033-0.4 Hz
Number of detection bands	19	11

Length of the detection window; frequency dependent	412.84-6.44 s	2555-118 s
Adjacent windows overlap	95 %	90 %
Consistency	0.1 s	3 s
Azimuth tolerance for families forming	10°	3°
Family size	10-50 pixels	15-50 pixels
Frequency range analysed in the study of streamer events	0.09-0.4 Hz	0.0033-0.4 Hz

238

239 **Table 2**. Main parameters of the DTK-GPMCC configurations for the arrays PVCI and

240 WBCI.

241

242 InfraGA/GeoAc raytracing tools are employed to study infrasound ducting in the

243 atmosphere (Blom and Waxler, 2012; Blom, 2019). Infrasound raytracing can reveal

244 possible modifications of atmospheric waveguides above the Eastern Atlantic and Western

245 Europe during streamer events. Streamer events influence the tropopause and lower

246 stratosphere. Hence, modifications of the stratospheric waveguide are expected rather than

247 its entire reversals or collapse. Raytracing can identify azimuths and distances from the

248 source that are influenced by a streamer event. And so, it can reveal whether these

249 influences reach Central Europe or the signals are ducted to the region through the

250 waveguide in the upper stratosphere or thermosphere like in quiet periods. InfraGA/GeoAc

251 provides simulations of signal propagation from a point source; propagation through the

252 range dependent atmosphere is modelled in the present study. Atmospheric characteristics

253 are obtained from the G2S model (Drob et al. 2003). Vertical profiles of temperature, zonal

254 and meridional winds, density and pressure are an input for the InfraGA/GeoAc. The grid

255 of profiles covers the area from 45° to 65°N and from 30°W to 22.5°E; latitudinal step is 5°

256 and longitudinal step is 7.5°.

257 Propagation of GW in the thermosphere/ionosphere is studied using the multi-point and multi-

258 frequency continuous Doppler sounding system located in Czechia. Its advantage is a high

259 time resolution (around 10 s) compared with ionospheric sounders (ionosondes) that measure

260 the profile of electron densities in the ionosphere. The frequency shift is due to the motion and

261 electron density changes in the ionospheric plasma, caused for example by interaction with

atmospheric waves propagating in the neutral atmosphere, with which the ionosphere (above

~ 80 km) merges. The sounding radio signal is reflected at the height, where its frequency

matches the so called local plasma frequency, which is determined by the local electron

density. Therefore, the reflection height changes during the day and depends on the sounding

frequency. Significant Doppler shifts, usable for analysis, are obtained if the signal is

reflected from the so called F2 layer (approximately 200 – 300 km). Several sounding

frequencies are used in Czechia. The 3.59 MHz sounding was mostly effective at night, while

the 4.65 MHz sounding provided good daytime data during the period analyzed. The

propagation characteristics of GWs are calculated from the time delays between signals

observed at the respective sounding paths (reflection points for each transmitter-receiver

pairs) assuming that the reflection points are in the midpoints between each transmitter and

receiver. A 60 or 90 min long time interval is usually used to calculate the velocities and

azimuth of the observed waves. The methods are in detail described by Chum and Podolska

(2018). The two-dimensional (2-D) version (propagation analysis in horizontal plane only) is

anticipated for most of the studies, since a 3-D analysis requires simultaneous observation and

signal correlation at different frequencies, which is often not the case, especially during solar

minimum. Results of statistical investigation have been recently published (Chum et al.,

2021). Identical methods of propagation analysis have been applied to investigate

propagation of GWs in the troposphere based on data from large-aperture array WBCI (here

the time delays are related to the locations of individual microbarometers). All analyses will

be done with respect to the streamer events and calm periods shown in Table 1.

3) Results

3.1 Infrasound observations at ground microbarograph arrays WBCI and PVCI in November 2020 and in March 2021

Wave activity in the infrasound frequency range of 0.0033-0.4 Hz is investigated combining

observations at the stations WBCI and PVCI. Infrasound detections at WBCI are processed in

the frequency band of 0.0033 – 0.4 Hz. The operational range of the array is extended above

the upper limit of the optimum array range; the degraded performance of WBCI at

frequencies higher than 0.0068 Hz shall be considered. The upper limit of the analysed band

is intentionally set to 0.4 Hz to cover microbaroms. PVCI detections are analysed in the

frequency range of 0.09 – 0.4 Hz. The band partly overlaps with the detection range of the

WBCI array and at frequencies of 0.12 – 0.35 Hz it is dominated by microbaroms (e.g.,

Campus and Christie, 2010). Unlike WBCI, PVCI provides an optimal performance in the microbarom band.

Microbaroms are infrasound signals generated by a non-linear interaction of ocean waves travelling in opposite directions. Microbaroms form a wide peak around 0.2 Hz in the infrasound spectrum; their frequency corresponds to twice the frequency of sea waves. A powerful source of microbaroms is located in the North Atlantic and the signals are regularly detected by European stations (Hupe et al., 2019). The detection capability of microbaroms from the North Atlantic is particularly high from October to March when the source becomes stronger due to stormy weather above the ocean and signal propagation to the East from the source is supported by the stratospheric waveguide (Landès et al., 2012). From the global point of view, microbaroms are permanently present in recordings of infrasound stations worldwide.

Streamer events often occur above the North Atlantic. Thus, microbaroms propagating from the North Atlantic to the continental Europe can travel through the region influenced by a streamer event and the detections at infrasound stations in Europe can show signatures of streamer events.

We analyse infrasound observations from 3rd to 25th November 2020 and from 28th February to 25th March 2021 with focus on microbaroms. In these time intervals adjacent streamers and calm periods occurred (Table 1). Streamers and the calm period in the November 2020 time window are evaluated separately from those in the March 2021 time window to avoid seasonal influences. While a well-developed eastward stratospheric waveguide can be expected in November, its efficiency can decrease in March due to the seasonal reversal of stratospheric winds.

### 3.1.1 Infrasound observations from 3rd to 25th November 2020

Two streamer events developed in November 2020. The first streamer occurred from 3rd to 7th November and the second one from 21st to 25th November. The streamers were separated by a calm period from 9th to 15th November.

The most important phenomena found in the infrasound arrival parameters are fluctuating signal frequency and fluctuating signal amplitude.

WBCI provides rather sparse detections during both streamer events and only two detection families are obtained during the seven-day calm period (Figure 3). The signal frequencies near 0.2 Hz and back-azimuths of 290° – 350° indicate that the observed signals are likely microbaroms from the North Atlantic. A decrease of the signal frequency

12

328   is observed during the first streamer event. On 5th – 6th November from 20 to 05 UTC, the

329   mean frequency of the north-west arrivals drops down to 0.04 Hz, below the microbarom

330   frequency range. During the second streamer event from 21st to 25th November, the signal

331   frequency is stable around 0.22 Hz. An increase of the amplitude from the mean value of

332   0.019 Pa to 0.035 Pa is observed from 23rd November, 18 UTC until the end of the analysed

333   time period on 25th November at 24 UTC.

334
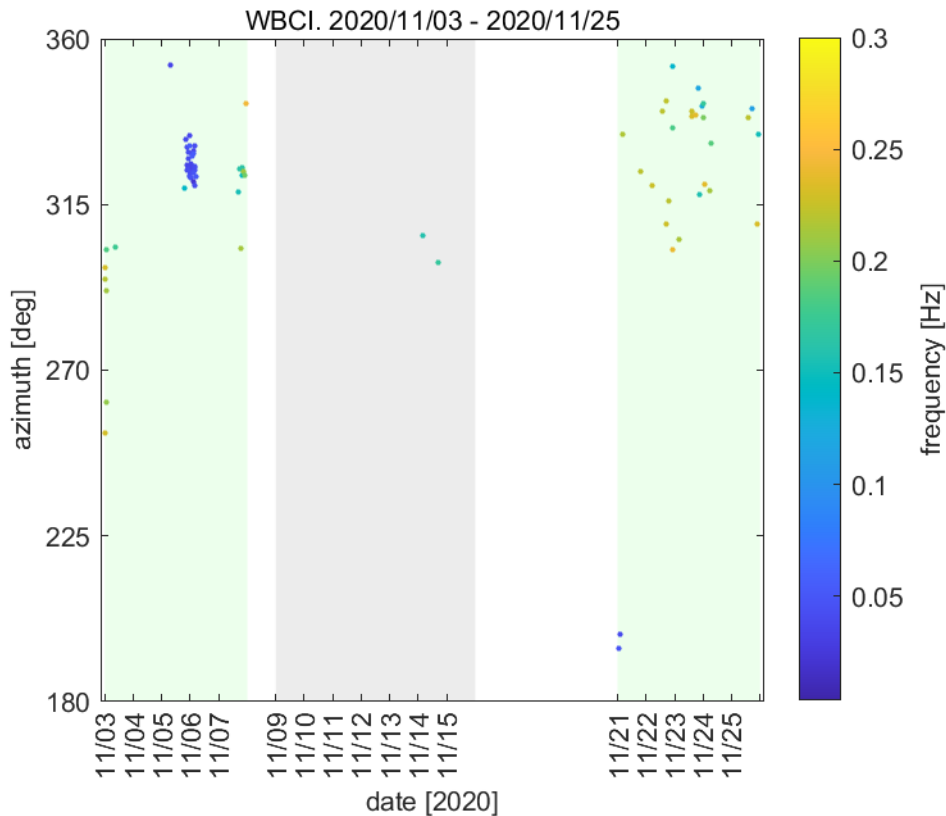
335

336   Fig. 3. Infrasound observations at WBCI on 3rd - 25th November 2020. Azimuth of signal

337   arrivals is shown; the colorbar refers to the mean frequency of the detection family. One circle

338   in the plot represents one detection family. Green background marks the streamer events, grey

339   background marks the calm period.

340

341   Similar to the back-azimuths at WBCI, PVCI detects arrivals from the north-west in the

342   analysed frequency range of 0.09 – 0.4 Hz (Figure 4). Fluctuating signal amplitudes are

343   observed. Values around 0.020 Pa occur on 3rd November. From 4th November, 18 UTC to

344   7th November, 22:30 UTC, the signals are of amplitudes around 0.089 Pa. The amplitudes

345   decrease to the values around 0.046 Pa during the following quiet period on 9th – 15th

346   November. Microbarom amplitudes fluctuate between 0.013 and 0.036 Pa (1st decile and 9th

13

decile, respectively) during the streamer event on 21st – 25th November. Publicly available data – meteorological charts provided by Deutscher Wetterdienst and the WAVEWATCHIII$^{®}$ wave-action model (The WAVEWATCHIII$^{®}$ Development Group, 2016) indicate that there are maritime storms in the North Atlantic within the analysed time window from 3rd to 25th November 2020. The storms can cause fluctuating intensity of the microbarom source and as a consequence, fluctuating microbarom amplitudes are observed at the infrasound stations.
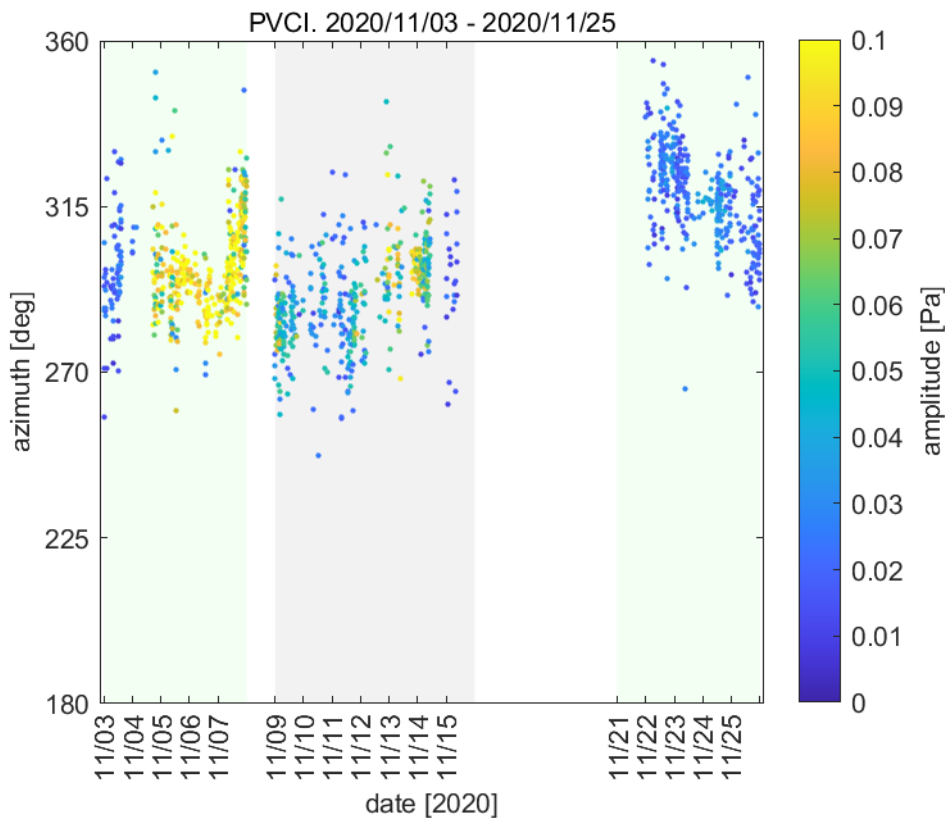
Fig.4. Infrasound observations at PVCI on 3rd - 25th November 2020. Azimuth of signal arrival is shown; the colorbar refers to the signal amplitude. Green background marks the streamer events, grey background marks the calm period.

To study propagation of signals from sources located at the surface of the North Atlantic the InfraGA/GeoAc tools are employed. The fictitious point sources are located (1) at 55°N and 15°W, (2) at 55°N and 5°W, and (3) at 60°N and 0°longitude. The coordinates of the sources are estimated based on the position of the tropopause jet stream disturbance. Point

(1) is located under the northward jet-stream, point (3) under the southward jet-stream, and point (2) is located between those two opposing branches of the jet stream disturbance see Figure 5.
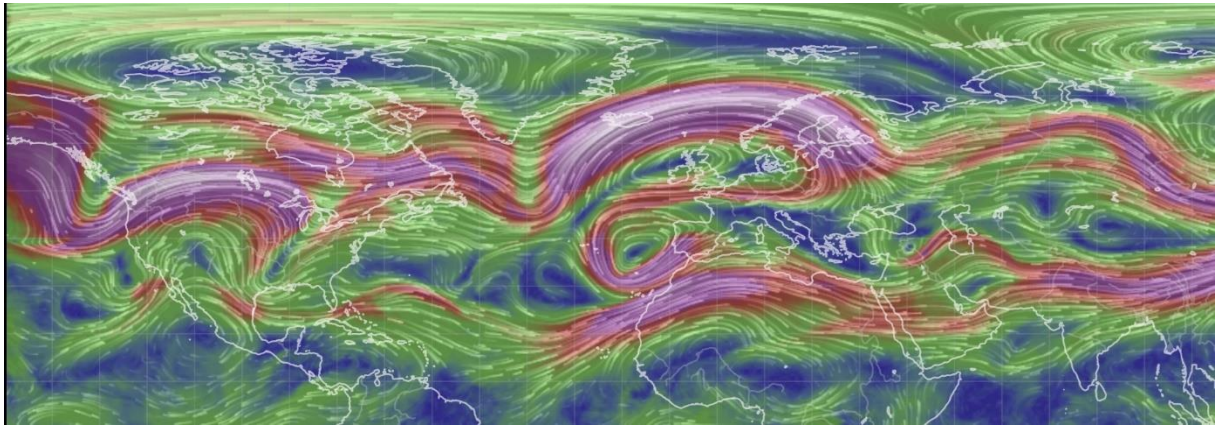
Fig.5. Wind field at the pressure level of *250 hPa* on 06 November 2020 at 00 UTC. A disturbance of the jet-stream above the eastern North Atlantic and the British Isles is caused by the streamer event.

A multi azimuth simulation is run on 6th November at 00 UTC, during the streamer event. Taking into account the mutual locations of the sources and the receiving arrays, eastward signal propagation is modelled. The azimuth limits are set to 0° and 180°, the azimuth step is 3°. Signal inclinations 2° – 45° are considered in 2° resolution. Information is obtained through which waveguides the signal can possibly arrive to the infrasound stations and their surroundings. The reason why arrivals to the larger areas are considered is that signal propagation from three fictious point sources stands in for an areal source, the surface of the North Atlantic where microbaroms are generated. Therefore, the model outputs must be taken as an approximation of the real situation. The turning height and ground reflections of the 0.2 Hz signal are obtained in the multi azimuth simulation. The results are visualised in Figure 6 and in supplementary materials. The red asterisk represents the point source. The concentric sectors of circles show regions of ensonification, regions where the signal emitted by the source can be recorded at an infrasound station. The dots, signal ground reflections are organized in a radial pattern. Each of the lines of this pattern represents one azimuth of signal propagation for which the multi azimuth simulation is run; the azimuth step is 3°. The colours of the dots inform about the turning height of the ray and thus provide information about signal ducting in the waveguides. Depending on the turning height, infrasound is subject to attenuation of variable strength when it propagates through

the atmosphere. Infrasound attenuation is low in the stratospheric waveguide. Strong absorption occurs in the thermospheric waveguide; the absorption is higher at higher signal frequencies (Sutherland and Bass, 2004). To obtain the view of signal attenuation along the raypath in the vertical plain a single azimuth simulation is employed. The single azimuth simulation is run along the azimuths from the fictitious sources (1) – (3) to the stations WBCI and PVCI; it is obtained for the frequencies of 0.04 Hz and 0.2 Hz. As a reference, a multi azimuth propagation of the 0.2 Hz signal is modelled from a source at 55°N and 15°W on the calm day 12th November at 00 UTC.

First, we focus on infrasound propagation from the North Atlantic to Central Europe. Stratospheric and thermospheric ducting are possible from the sources at 55°N 15°W and 55°N 5°W to Central Europe during the streamer event as well as on the calm day (supplementary materials). Signal propagation only through the thermospheric waveguide is enabled from the source at 60°N and 0°longitude (Figure 6). The distances between the fictitious sources and the stations are 1300 – 2000 km. The amplitude loss of the 0.2 Hz signal in the thermospheric waveguide at these distances is 100 dB relative to the amplitude at a distance of 1 km from the source. According to the simulations, observations of the thermospheric arrivals of microbaroms are unlikely at PVCI and WBCI due to strong signal attenuation. Microbaroms apparently arrive to Central Europe through the waveguide formed in the upper stratosphere during the streamer events as well as on the calm day. Indeed, arrivals from the back-azimuths of 285° - 315° are dominant at PVCI o 3rd to 7th November. Those back-azimuths correspond to the sources at 55°N 15°W and at 55°N 5°W, while the back-azimuth to the source at 60°N and 0°latitude is 325°. The amplitude loss of the 0.04 Hz signal at the distances of 1300 – 2000 km from the source is 60 – 80 dB. In general, thermospheric arrivals of this low frequency signal are not strictly rejected. However, in our case the 0.04 Hz signal arrives with trace velocity around 0.330 km/s at WBCI. The low trace velocity indicates signal ducting in the troposphere/lower stratosphere waveguide (Lonzaga, 2015).

Next, we study the influences of the streamer event related disturbance anywhere in the modelled region. The disturbance of the jet stream can modify signal propagation up to distances of several hundreds to a thousand km from the source; the influenced azimuth range is limited. Signals from the source at 55°N and 15°W can propagate in the tropopause waveguide in azimuths between 10° and 60° up to the distance of ~1000 km. The amplitude loss of the 0.2 Hz signal at a distance of 1000 km is 60-70 dB relative to the amplitude at 1 km from the source. The southward branch of the jet-stream disturbance enables infrasound

propagation in the tropospheric waveguide in azimuths of 100 - 160° from the source at 60°N 0°longitude. Maximum distance which the signal can travel in the south-east direction is ~600 km. The amplitude loss of the 0.2 Hz signal at a distance of 600 km is 60 dB relative to the amplitude at 1 km from the source.

The observations and the model outputs during the November 2020 event can be summarized as follows: infrasound arrives from sources in the North Atlantic to Central Europe mainly through the stratospheric waveguide formed between the ground and upper stratosphere. The jet-stream disturbance above the eastern North Atlantic does not have an impact on infrasound arrivals in Central Europe on 6th November 2020 at 00 UTC. Fluctuating signal amplitudes are likely a consequence of fluctuating intensity of the microbarom source during maritime storms. The decrease of signal frequency at WBCI is not caused by a transient change in signal ducting and by the related signal filtering in the thermospheric waveguide.
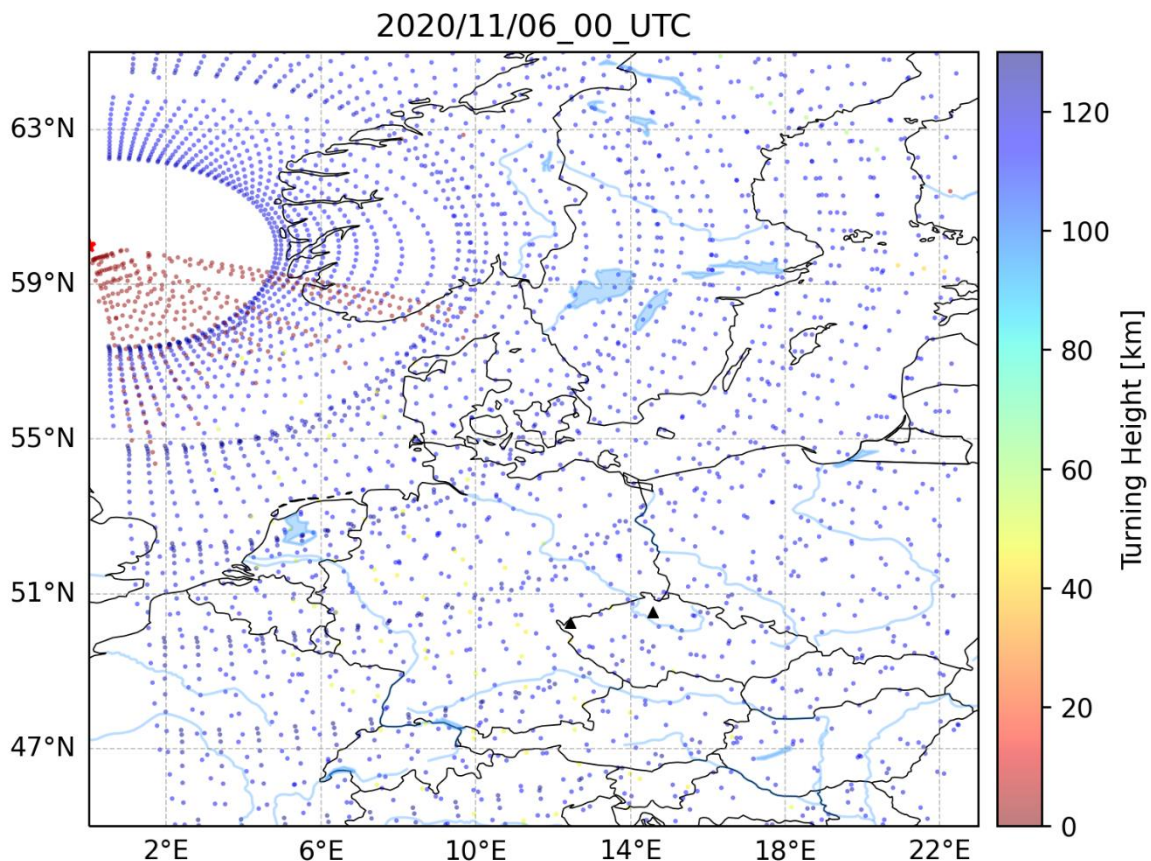
Fig.6. Modelled infrasound propagation from a point source located at 60°N and 0°longitude (red asterisk) during the streamer event on 6th November 2020 at 00 UTC. Colobar refers to the turning height (maximum height) of the signal. Red indicates signal propagation in the

waveguide formed near the tropopause (altitudes around 10 km), arrivals through the thermospheric waveguide are in blue (altitudes above 100 km). Black triangles represent infrasound arrays WBCI (the left triangle) and PVCI (the right triangle).

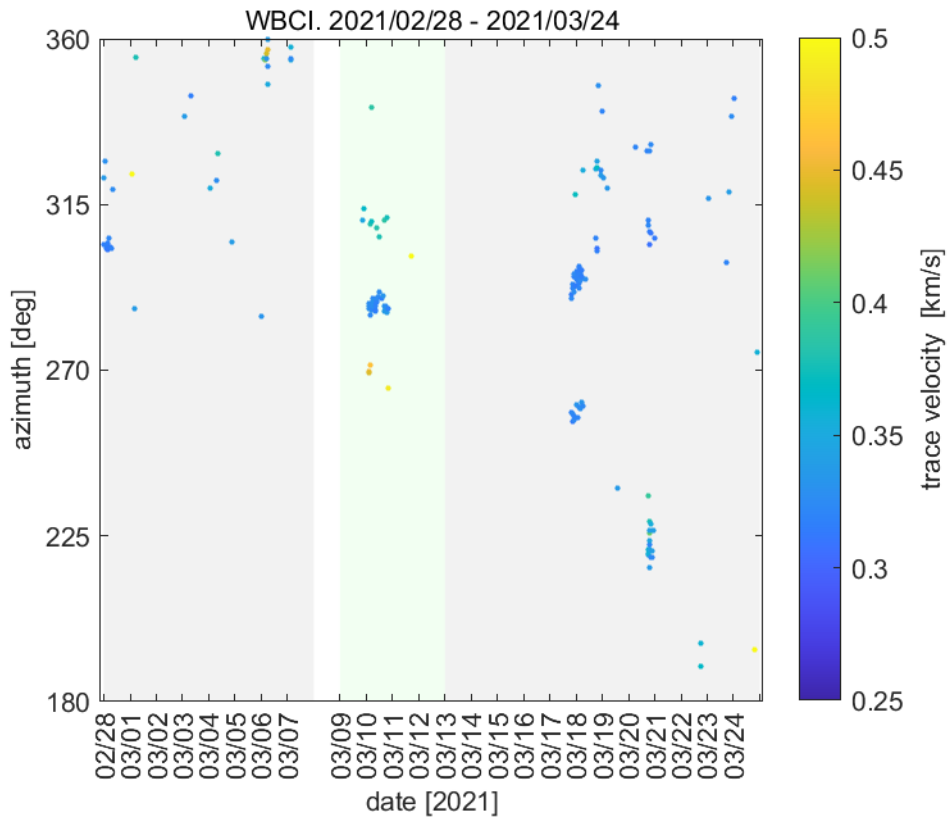### 3.1.2 Infrasound observations from 28th February to 24th March 2021

A streamer event occurred from 9th to 12th March 2021 preceded and followed by calm periods from 28th February to 7th March and from 13th to 24th March, respectively.

The most important phenomenon identified in the infrasound arrival parameters is a fluctuating trace velocity.

Both WBCI and PVCI detect signals arriving from the north-west, from back-azimuths of 285° – 310°. An increase of signal trace velocities is observed in some of the detections at WBCI during the streamer event compared to calm periods (Figure 7). On 10th March at 00 – 06 UTC, trace velocities of 0.460 km/s and 0.380 km/s are observed from back-azimuths of 270° and 310° respectively. It is by 0.05 – 0.13 km/s higher than on the calm days. On the other hand, signals from the back-azimuth of 288° arrive with the trace velocity of 0.330 km/s within the same time window, the velocity corresponds to that on the calm days. Effects of spatial aliasing shall be taken into account when evaluating the detections. The signal frequencies are around 0.2 Hz, well above the range of array optimum performance. The observed different trace velocities at WBCI can therefore be a processing bias rather than a consequence of variations in signal ducting.

In contrast to the WBCI observations, PVCI records a decrease in trace velocities on 10th March at 00 – 06 UTC (Figure 8). Trace velocities of 0.377 km/s are observed compared to 0.413 km/s and 0.395 km/s during the calm periods before and after the streamer, respectively.

18

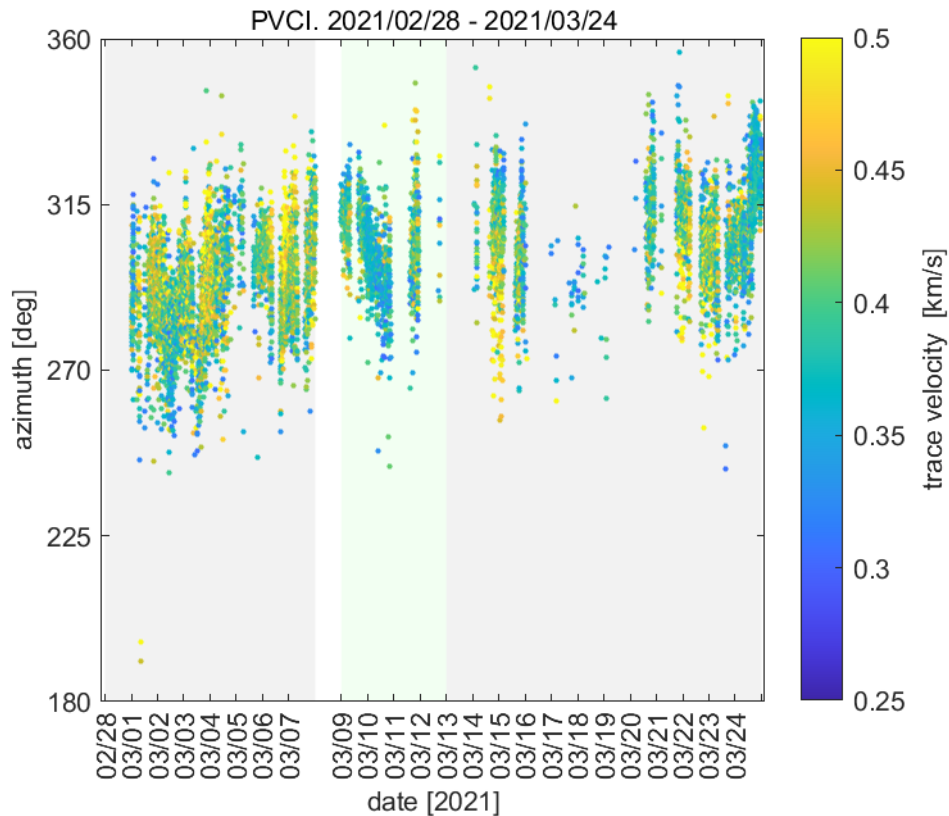Fig.7. Infrasound observations at WBCI on 28th February – 24th March 2021. Azimuth of signal arrival is shown; the colorbar refers to the signal trace velocity. Green background marks the streamer event, grey background marks the calm periods.

Fig.8. Infrasound observations at PVCI on 28th February – 24th March 2021. Azimuth of signal arrival is shown; the colorbar refers to the signal trace velocity. Green background marks the streamer event, grey background marks the calm periods.

Changes of the trace velocity can indicate changes of the refraction altitude of the signal (Lonzaga, 2015). The exact limits of the trace velocity for the given atmospheric waveguide depend on the current state of the atmosphere. We use the thresholds determined for a model atmosphere in Lonzaga (2015) as helpful hints for our further consideration: Trace velocities below 0.340 km/s indicate signal refraction in the troposphere and lower stratosphere. Trace velocities between 0.340 and 0.380 km/s are typical for signals ducted in the waveguide between the ground and the upper stratosphere. Signals traveling in the thermospheric waveguide arrive with trace velocities larger than 0.380 km/s.

The high trace velocities recorded at PVCI disprove signal refraction in the lower stratosphere. Hence, it is unlikely that the signals arrive through a waveguide that can form at the tropopause – lower stratosphere by the effect of the streamer event.

Like in the November 2020 case, signal propagation above the eastern North Atlantic and Western and Central Europe is investigated using the InfraGA/GeoAc tools. Propagation of the 0.2 Hz signal is modelled on 10th March at 03 UTC. A source is located at 55°N 15°W

at a distance of ~2000 km from the stations. This scenario represents signal propagation from the central North Atlantic. The other source is located at 55°N 0°latitude representing propagation of microbaroms from the North Sea. The distance from the stations is ~1000 km.

Eastward signal ducting is enabled in the stratospheric and thermospheric waveguides from both sources to the stations. Strong signal absorption in the thermospheric waveguide likely disables thermospheric arrivals to the PVCI and WBCI. We assume that signals ducted in the upper stratosphere are detected. The other eastward waveguide occurs near the tropopause, formed by the eastward to south-eastward jet-stream above the eastern North Atlantic and Western Europe at latitudes 50 – 60°N Figure 9. Signals from the source in the North Atlantic are predicted to travel in the tropopause waveguide to distances of 1000-1100 km. The signal attenuation is low in the tropopause waveguide; the relatively short distance under the waveguide influence is determined by the location and extent of the jet-stream disturbance. The tropopause/lower stratosphere arrivals can be detected mainly on the British Isles. The waveguide does not reach to PVCI and WBCI stations (see supplementary materials).

Signals emitted by a source in the North Sea can propagate through the tropopause waveguide. The signals propagate to the south-east and are predicted to reach Central Europe. The tropopause/lower stratosphere arrivals are represented by red dots in Figure 10. The influenced regions are to the south-west from PVCI and WBCI, several hundreds of kilometres distant from the stations. The approximation of infrasound propagation obtained from the raytracing is in accord with observations. The trace velocities at PVCI of 0.377 km/s indicate infrasound propagation in the waveguide formed between the ground and the upper stratosphere rather than in the waveguide near the tropopause.

Like in the November 2020 case, infrasound arrivals from the North Atlantic to the stations PVCI and WBCI in Central Europe are not influenced by the waveguide at the tropopause – lower stratosphere. Observed trace velocities fluctuate within or close above the limits that indicate infrasound propagation in the upper stratosphere during the streamer event and both adjacent quiet periods.
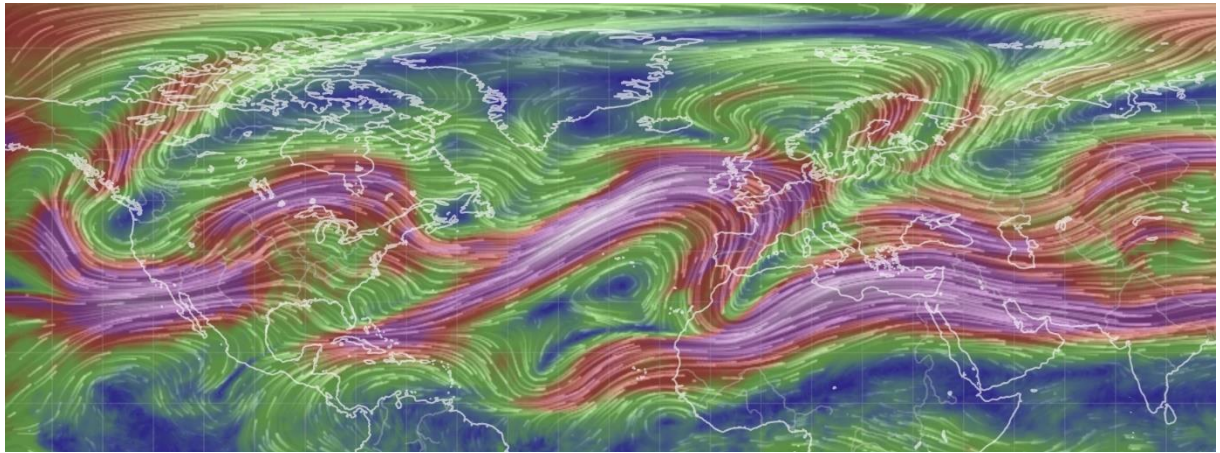
Fig.9. Wind field at the pressure level of *250 hPa* on 10 March 2021 at 03 UTC. A
disturbance of the jet-stream above the eastern North Atlantic and the British Isles is caused
by the streamer event.
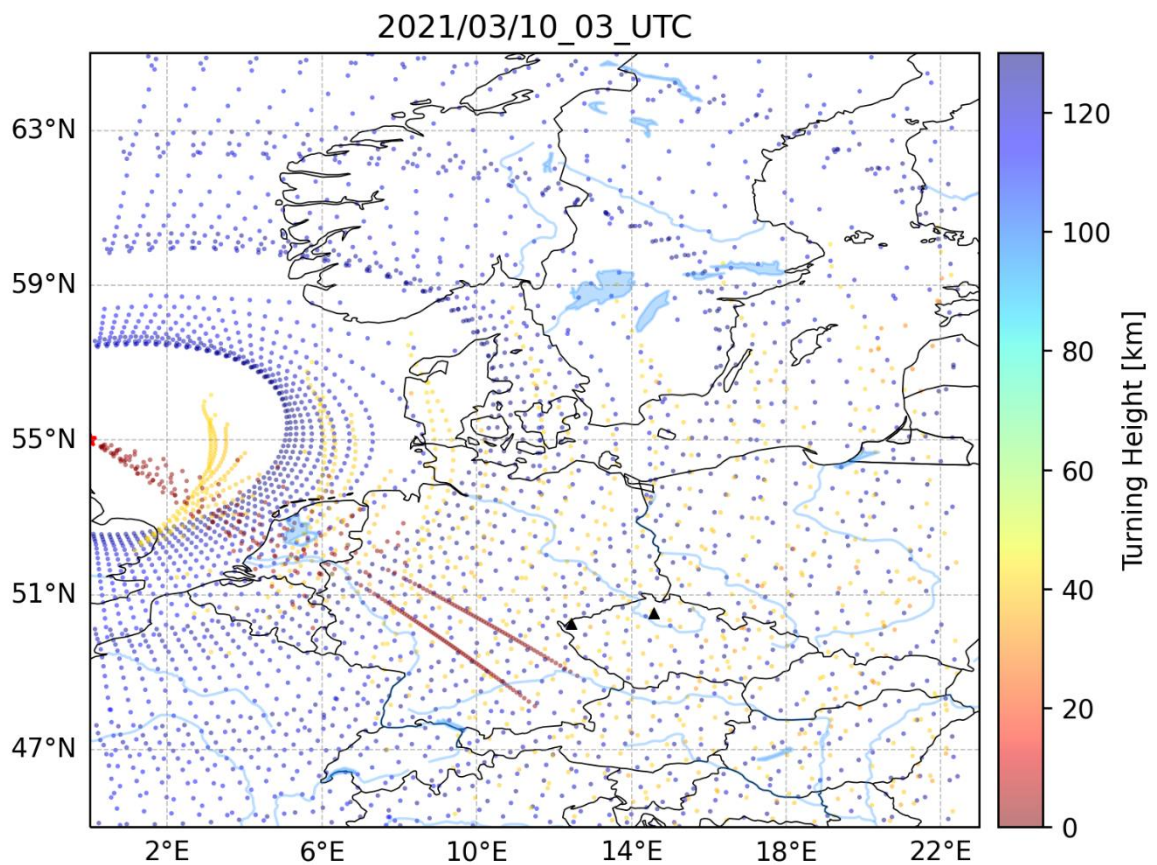
Fig.10 Modelled infrasound propagation from a point source located at 55°N and 0°longitude
(red asterisk) on 10th March 2021 at 03 UTC. Colobar refers to the turning height (maximum
height) of the signal. Red indicates signal propagation in the waveguide formed near the
tropopause (altitudes around 10 km), arrivals through the stratospheric waveguide are in

yellow (altitudes around 40-50 km) and arrivals through the thermospheric waveguide are in blue (altitudes above 100 km). Black triangles represent infrasound arrays WBCI (the left triangle) and PVCI (the right triangle).

### 3.2 Results and discussion of gravity waves in the troposphere and ionosphere

3.2.1 **Investigation of GWs measured on the ground by WBCI array of micro-barometers**.

Figure 12 shows the RMS amplitudes of pressure fluctuations in the period range 5-60 min recorded from November 1 to November 9, 2020. This interval covers a distinct streamer event that occurred from November 3 to November 7. The results of propagation analysis are shown in Figure 13, which displays the phase velocities and azimuths of GWs. Only results that satisfied the criterion (dv/v <0.5) and (dAZ<10°) and (p_{RMS}>0.02 Pa) are presented, where dv/v, dAZ, p_{RMS} are the relative uncertainty of GW phase velocity, uncertainty of azimuth and root mean square value of pressure fluctuations in the analysed time interval. Figure 13 demonstrates that there is a tendency for higher phase velocities and occurrence of different azimuths during the streamer event. Therefore, it is useful to compare the GW characteristics during streamer events and calm conditions.

Figure 14 shows histograms obtained by a statistical analysis. The RMS amplitudes of pressure fluctuations in the period range 5 – 60 min, phase velocities and azimuths were investigated separately for calm conditions (upper plots) and for streamer events listed in Table 1 (bottom plots) with a 1-hour time resolution. The solid vertical lines mark lower (Q1) and upper (Q3) quartiles. The dashed vertical lines depict boundaries for large (Q3+1.5·(Q3-Q1)) and extreme (Q3+3·(Q3-Q1)) values. A difference between histograms for RMS pressure fluctuations and azimuths obtained for calm and disturbed conditions is obvious. During the streamer events the azimuths are distributed more randomly and more extreme pressure amplitudes can be observed. A minor difference is also observed for phase velocities.

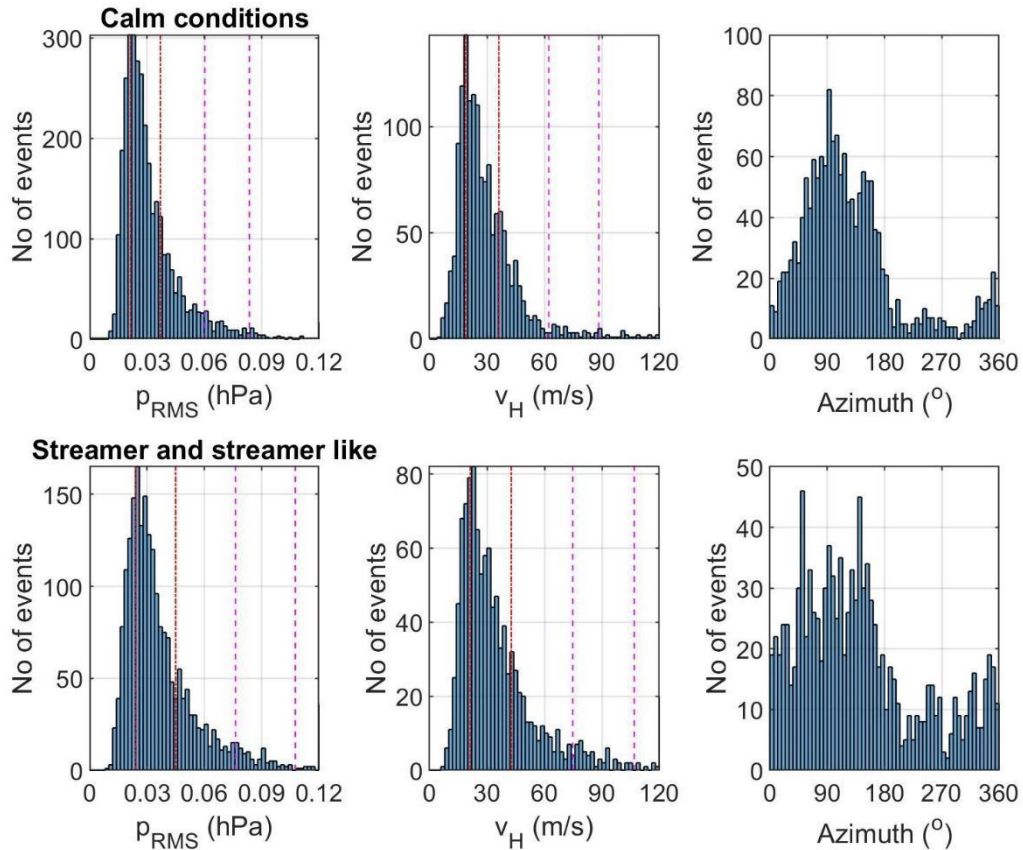RMS value of pressure fluctuations in the period range 5 - 60 min
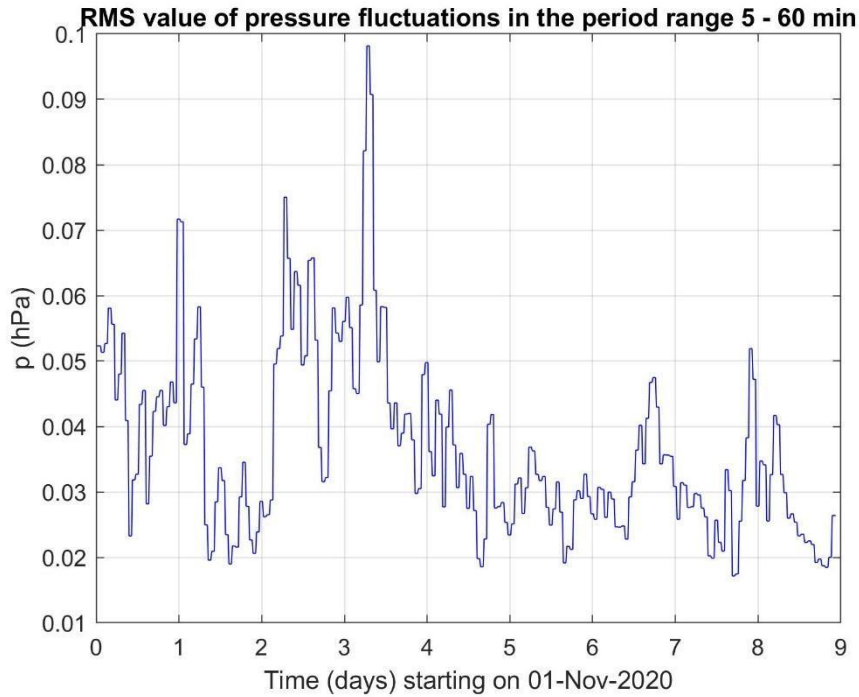
563

564   **Figure 12** Amplitude of GWs recorded by WBCI from 2020-11-01 to 2020-11-09
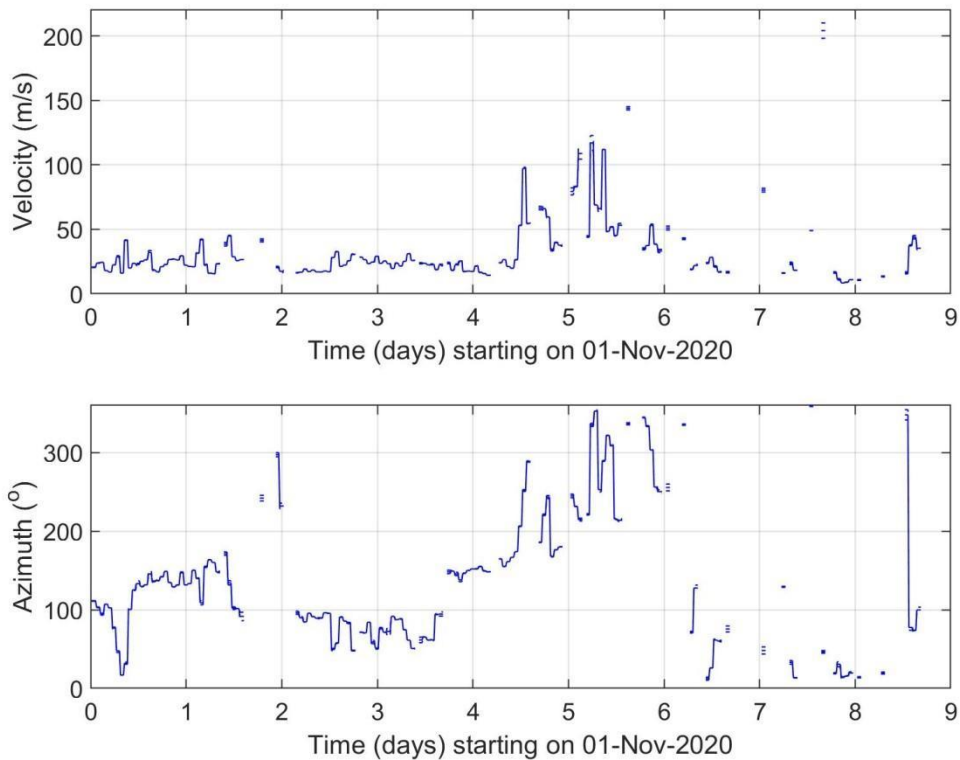
565

566   **Figure 13** Propagation velocity and azimuth of GWs recorded by WBCI from 2020-11-01 to

567   2020-11-09

Figure 14 GW characteristics (RMS of pressure fluctuations, phase velocity and azimuth) for calm periods (upper plots) and streamer and streamer like events (bottom plots) for 2020 and winter 2021. The red vertical lines mark lower (Q1) and upper (Q3) quartiles. The dashed magenta vertical lines depict boundaries for large (Q3+1.5·(Q3-Q1)) and extreme (Q3+3·(Q3-Q1)) values.

3.2.2 Investigation of GWs measured in the ionosphere by continuous Doppler sounding system (CDS)

The 2D propagation analysis of GWs was performed using the 2D versions of methods mentioned in Section 2 and in detail described by Chum and Podolská (2018). As discussed in Section 2 and by (Chum et al., 2021), the 2D propagation analysis makes it possible to analyze much larger number of time intervals than the 3D analysis. The propagation analysis obtained for the interval from 1st November to 9th November 2020, which covers the significant streamer event that occurred from 3rd November 2020 to 7th November 2020, is presented in Figure 15. Only results that satisfied the criteria (dv/v <0.2) and (dAZ<20°) and

584 (f_{DRMS}>0.05 Hz) and (C_{max}<0.5) are presented, where dv/v is the relative uncertainty of GW

585 phase velocity, dAZ is the azimuth uncertainty, f_{DRMS} is the root mean square of the Doppler

586 shift in the analysed time interval and C_{max} is the maximum in the normalized energy map for

587 the best beam (slowness) search; C_{max} is 1 for identical signals (Chum and Podolská, 2018). It

588 is considered that signals are not sufficiently correlated (coherent) for reliable propagation

589 analysis if $C_{max} < 0.5$ (Chum et al., 2021). The velocities and azimuth obtained by observation

590 at 3.59 MHz are in red, whereas the values based on measurements at 4.65 MHz are in blue.

591 Obviously, the observations at 3.59 MHz mostly correspond to the nighttime, whereas

592 observations at 4.65 MHz were mostly made during the daytime. The 4.65 MHz signal did not

593 reflect from the ionosphere (escaped to the outer space) at night due to the low critical

594 frequency of the ionosphere. On the other hand, the 3.59 MHz signal mostly reflected during

595 the day from the ionospheric E layer and the Doppler shift was negligible, difficult to

596 analyse.The GWs usually propagated roughly poleward at night and roughly equatorward

597 during the daytime. This is fully consistent with the statistical investigation (Chum et al.,

598 2021) which showed that propagation directions of GWs in the ionosphere exhibit diurnal and

599 seasonal behaviour and are mainly controlled by the neutral winds in the thermosphere.

600
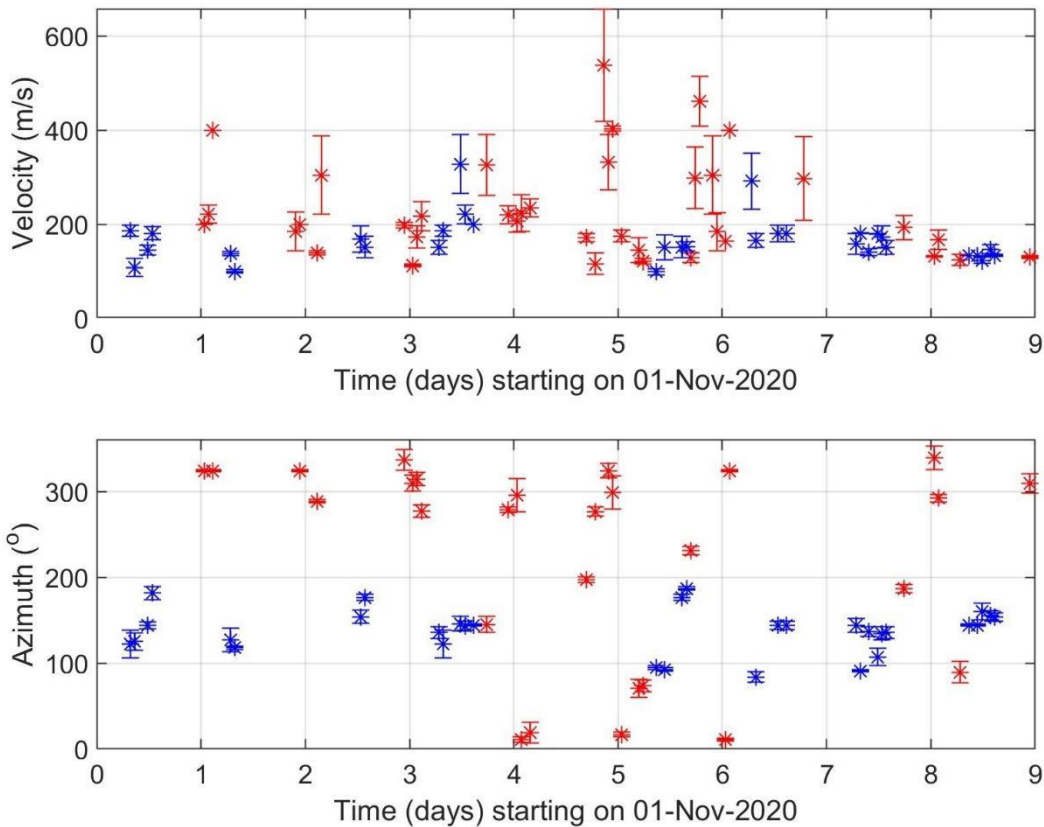
Figure 15 Propagation velocity and azimuth of GWs in the ionosphere obtained using CDS measurements from 2020-11-01 to 2020-11-09. The velocities and azimuth obtained by observation at 3.59 MHz are by red, whereas the values based on measurements at 4.65 MHz are by blue.

Based on the analysis of the GW observed in the ionosphere during the streamer event and on the previous statistical analysis, we conclude that no obvious signature related to streamer event was observed for the propagation of GW the ionosphere.

It should be also mentioned that the phase velocities of GW measured on the ground (Figure 8) and at heights around 200 km in the ionosphere differ. There are several reasons for that. First, the observed horizontal phase velocities depend on the elevation angle of GW propagation and on the ambient temperature as follows from the dispersion relation (the temperature enters the dispersion relation via the buoyancy frequency and the scale height). The temperature in the ionosphere/thermosphere is several times higher than in the troposphere. The elevation angles might change during the upward propagation of GWs, depending on the wind and temperature profile. Second, GWs propagate with a tilt, not vertically upward. It is therefore highly probable that the sources of the GWs observed in the troposphere and ionosphere are different. Moreover, GW can break during their propagation upward and secondary gravity waves might be observed in the ionosphere.

4) Conclusion and discussion

The focus of this study was to test independent types of observations like Doppler sounding and microbarograph measurements for an analysis of GW behavior during streamer events, which are strongly connected with PW or GW and the large scale mass transport of ozone and that is why it can be very interesting for studies of atmospheric dynamics.

We also investigate effects of the streamer events on infrasound propagation. Streamer events are significant disturbances to circulation in the tropopause/lower stratosphere region. Modifications of infrasound ducting in the atmosphere can therefore be expected. Indeed, the InfraGA/GeoAc raytracing tools predict that a waveguide develops at the tropopause during the analyzed streamer events in November 2020 and in March 2021 the direction of which is determined by the disturbed jet-stream and varies from event to event. The tropopause waveguide ducts infrasound up to distances of several hundreds to a thousand of km from the source in a limited azimuth range. The azimuth sector of the extent of 50 – 60° is influenced in the analysed cases. In accord with the model predictions, streamer event related phenomena

27

were not found in infrasound detection at the infrasound stations PVCI and WBCI in Central Europe during the studied cases. The observability of streamer event signatures in infrasound arrival parameters therefore strongly depends on the mutual position of the source, the streamer event disturbance of the tropopause jet-stream and the infrasound station. It can be recommended for future studies to use a dense network of infrasound arrays that covers various directions and distances from the streamer event. Due to the typical occurrence of the streamer events over the North Atlantic, infrasound stations in Western Europe can be of particular interest.

Supplementary ground-based measurements of GW using the WBCI array in the troposphere showed that GW propagation azimuths were more random during streamer and streamer-like events compared to those observed during calm conditions as can be seen from the plots in Figure 14. On the other hand, the GW propagation characteristics observed in the ionosphere by CDS during streamer events did not differ from those expected for the given time period, based on previous statistical studies (Chum et al., 2021).

The results therefore indicate that streamers in the stratosphere might lead to changes in wave propagation in the troposphere. The impact on the ionosphere was not confirmed, but cannot be excluded due to spare and localized observations of GW activity. In general, to validate the preliminary results obtained in this study, a denser measurement network and more streamer events need to be analyzed.

Data availability:

ozone column measurements (TO3) which are available as a service by DLR at

https://atmos.eoc.dlr.de/

Ground to space model vertical atmospheric profiles were obtained at

https://g2s.ncpa.olemiss.edu/; accessed on 27 January – 4 February 2024

The WAVEWATCHIII® wave-action model data were accessed via ftp at

polar.ncep.noaa.gov/waves/JCOMM/2020 on 13-14 March 2023.

662 The Deutscher Wetterdienst synoptic charts were accessed at

663 https://www2.wetter3.de/archiv_dwd_dt.html on 3 February 2024.

664

665 **Author contributions**
666 MK and LK create the idea of manuscript; JCh, MK, TS, LK, and KP suggest the datasets and
667 methods; TS, JCh, LK, KP and FT analyzed the data; MK wrote the manuscript draft; JCh,
668 TS, LK and KP reviewed and edited the manuscript.

669 **Competing interests**
670 The authors declare that they have no conflict of interest.

671

681

682   **References**

683 Assink, J.D., Waxler, R., Smets, P., Evers, L.G. (2014). Bidirectional infrasonic ducts

684 associated with sudden stratospheric warm-ing events. J. Geophys. Res. Atmos. 119,1140-

685 1153.

686 Bittner, M., Höppner, K., Pilger, C., Schmidt, C. (2010). Mesopause temperature

687 perturbations caused bzy infrasonic waves as a potential indicator for the detection of

688 tsunamis and other geo-hazards. Nat. Hazards Earth Syst. Sci., 10, 1431-1442. www.nat-

689 hazards-earth-syst-sci.net/10/1431/2010/doi:10.5194/nhess-10-1431-2010

690 Blanc, E. (1985). Observations in the upper atmosphere of infrasonic waves from natural or

691 artificial sources: A summary. Ann. Geophys., 3, 673-688.

692   Blixt, E.M., Nasholm, S.P., Gibbons, S.J., Evers, L.G., Charlton-Perez, A.J., Orsolini, Y.J.,

693   Kvaerna, T. (2019). Estimating tropo-spheric and stratospheric winds using infrasound from

694   explosions. J. Acoust. Soc. Am. 146:2.

695   Blom, P., Waxler, R. (2012). "Impulse propagation in the nocturnal boundary layer: Analysis

696   of the geometric component". *J. Acoust. Soc. Am.,* **131**, 3680 – 3690. doi:

697   10.1121/1.3699174.

698   Blom, P. (2019). "Modeling infrasonic propagation through a spherical atmospheric layer:

699   Analysis of the stratospheric pair*." J. Acoust. Soc. Am.,* **145**, 2198–2208. doi:

700   10.1121/1.5096855.

701   Bondár I., T. Šindelářová, D. Ghica, U. Mitterbauer, A.Liashchuk, J. Baše, J. Chum, C.

702   Czanik, C. Ionescu, C. Neagoe, M. Pásztor, A. Le Pichon (2022), Central and Eastern

703   European Infrasound Network: Contribution to Infrasound Monitoring, *Geophys. J. Int.*,

704   ggac066, https://doi.org/10.1093/gji/ggac066

705   Brachet, N., Brown, D., Le Bras R., Cansi, Y., Mialle, P., Coyne, J. (2010). Monitoring the

706   Earth's Atmosphere with the Global IMS Infrasound Network. In: Le Pichon, A., Blanc, E.,

707   Hauchecorne A. (Eds.), Infrasound Monitoring for Atmospheric Studies. Springer

708   Science+Business Media B.V., 77-118. Doi: 10.1007/978-1-4020-9508-5_3

709   Campus, P., Christie, D.R. (2010). Worldwide Observations of Infrasonic Waves. In: Le

710   Pichon, A., Blanc, E., Hauchecorne A. (Eds.), Infrasound Monitoring for Atmospheric

711   Studies. Springer Science+Business Media B.V., 185234-118. Doi: 10.1007/978-1-4020-

712   9508-5_6

713   Cansi, Y., 1995. An automatic seismic event processing for detection and location: The

714   P.M.C.C. method. Geophys. Res. Lett. 22, 1021-1024. doi: 10.1029/95GL00468

715   Ceranna, L., Matoza, R., Hupe, P., Le Pichon, A., Landès, M., (2019). Systematic Array

716   Processing of a Decade of Global IMS Infrasound Data. In: Le Pichon, A., Blanc, E.,

717   Hauchecorne, A. (eds) Infrasound Monitoring for Atmospheric Studies. Chal-lenges in

718   Middle Atmospheric Dynamics and Societal Benefits. Springer Nature Switzerland AG.

719   Chum J, Podolská K (2018) 3D analysis of GW propagation in the ionosphere. Geophysical

720   Research Letters, 45, 11,562–11,571, https://doi.org/10.1029/2018GL07969

721 Chum, J., Podolská, K., Rusz, J., Baše, J., Tedoradze, N. (2021), Statistical investigation of

722 gravity wave characteristics in the ionosphere. Earth Planets Space 73, 60,

723 https://doi.org/10.1186/s40623-021-01379-3

724 Czech microbarograph network, https://doi.org/10.7914/SN/C9

725 Drob, D. P., Picone, J. M., Garcés, M. (2003). Global morphology of infrasound propagation.

726 *J. Geophys. Res. Atmospheres*, **108** (D21). doi: 10.1029/2002JD003307.

727 Evers, L. G., Siegmund, P. (2009). Infrasonic signature of the 2009 major sudden

728 stratosphericwarming, Geophys. Res. Lett., 36, L23808, doi:10.1029/2009GL041323

729 Evers, L.G., Haak, H.W. (2010). The Characteristics of Infrasound, its Propagation and Some

730 Early History. In: Le Pichon, A., Blanc, E., Hauchecorne, A. (eds) Infrasound Monitoring for

731 Atmospheric Studies. Springer, Dordrecht.

732 Evers, L. G., van Geyt, A. R. J. , Smets, P., Fricke, J.T. (2012). Anomalous infrasound

733 propagation in a hot stratosphere and the existence of extremely small shadow zones, J.

734 Geophys. Res., 117, D06120, doi:10.1029/2011JD017014.

735

736 Eyring, V., Dameris, M., Grewe, V., Langbein, I., & Kouker, W. (2002). Climatologies of

737 streamer events derived from a transport model and a coupled chemistry-climate model.

738 Fritts, D.C. & Alexander, M.J., (2003). Gravity wave dynamics and effects in the middle

739 atmosphere. Rev. Geophys., 41 (1), 1003.

740 Garcès, M., Willis, M., Hetzer, C., Le Pichon , A., Drob, D., (2004). On using ocean swells

741 for continuous infrasonic measurements of winds and temperature in the lower, middle, and

742 upper atmosphere. Geophys. Res. Lett. 31, L19304. doi: 10.1029/2004GL020696

743 Garcès, M.A., (2013). On infrasound standards, part 1: Time, frequency, and energy scaling.

744 InfraMatics 2, 13-35. doi: 10.4236/inframatics.2013.22002

745 Georges, T.M. (1968). H. F. Doppler studies of travelling ionospheric disturbances. J.

746 Atmos.Terr. Phys., 30, 735-746.

747   Gerlach, C., Földvary, L., Švehla, D., Gruber, T., Wermuth, M., Sneeuw, N., ... &

748   Steigenberger, P. (2003). A CHAMP-only gravity field model from kinematic orbits using the

749   energy integral. Geophysical Research Letters, 30(20).

750   Hersbach, H., Bell, B., Berrisford, P., Hirahara, S., Horányi, A., Muñoz-Sabater, J., ... &

751   Thépaut, J. N. (2020). The ERA5 global reanalysis. Quarterly Journal of the Royal

752   Meteorological Society, 146(730), 1999-2049.

753   Hupe, P., Ceranna, L., Pilger, C., de Carlo, M., Le Pichon, A., Kaifler, B., Rapp, M. (2019).

754   Assessing middle atmosphere weather models using infrasound detections from microbaroms.

755   Geophys. J. Int., 216, 1761–1767 doi: 10.1093/gji/ggy520

756   James, P. M. (1998): A climatology of ozone mini-holes over the Northern Hemisphere.

757   International Journal of Climatology: A Journal of the Royal Meteorological Society, 18, 12:

758   12871303

759   Kramer, R, S. Wüst, and M. Bittner (2016). Investigation of gravity wave activity based on

760   operational radiosonde data from 13 years (1997-2009): Climatology and possible induced

761   variability, Journal of Atmospheric and Solar-Terrestrial Physics 140, 23–33;

762   http://dx.doi.org/10.1016/j.jastp.2016.01.014

763   Kramer, R., S. Wüst, C. Schmidt, and M. Bittner (2015). Gravity wave characteristics in the

764   middle atmosphere during the CESAR campaign at Palma de Mallorca in 2011/2012: Impact

765   of extratropical cyclones and cold fronts, Journal of Atmospheric and Solar-Terrestrial

766   Physics 128 (2015) 8–23, http://dx.doi.org/10.1016/j.jastp.2015.03.001

767   Kai Ming Huang, Shao Dong Zhang, Fan Yi, (2010).Reflection and transmission of

768   atmospheric gravity waves in a stably sheared horizontal wind field, Journal of Geophysical

769   Research: Atmospheres, 10.1029/2009JD012687, **115**, D16,

770   Landès, M., Ceranna, L., Le Pichon, A., & Matoza, R. S. (2012). Localization of microbarom

771   sources using the IMS infrasound network. Journal of Geophysical Research:

772   Atmospheres, 117(D6).

773   Le Pichon, A., Cansi, Y. (2003). PMCC for infrasound data processing. InfraMatics 02, 1-9.

774   Le Pichon, A., Blanc, E., (2005). Probing high-altitude winds using infrasound. J. Geophys.

775   Res., 110, D20104. doi: 10.1029/2005JD006020

776   Le Pichon, A., Ceranna, L., Garcès, M., Drob, D., Millet, C., (2006). On using infrasound

777   from interacting ocean swells for global continuous measurements of winds and temperature

778   in the stratosphere. J. Geophys. Res., 111, D11106. doi: 10.1029/2005JD006690

779   Le Pichon, A., Vergoz, J., Blanc, E., Guilbert, J., Ceranna, L., Evers, L., Brachet, N., (2009).

780   Assessing the performance of the International Monitoring System's infrasound network:

781   Geographical coverage and temporal variabilities. J. Geophys. Res. 114, D08112. doi:

782   10.1029/2008JD010907

783   Leovy, C. B., Sun, C. R., Hitchman, M. H., Remsberg, E. E., Russell III, J. M., Gordley, L.

784   L., ... & Lyjak, L. V. (1985). Transport of ozone in the middle stratosphere: Evidence for

785   planetary wave breaking. Journal of Atmospheric Sciences, 42(3), 230-244.

786   Lonzaga, J.B., (2015). A theoretical relation between the celerity and trace velocity of

787   infrasonic phases, J. Acoust. Soc. Am., 138, EL242-EL247.

788   http://dx.doi.org/10.1121/1.4929628

789   Loyola D.G., Koukouli M.E., Valks P., Balis D.S., Hao N., van Roozendael M., Spurr R.J.D.,

790   Zimmer W., Kiemle S., Lerot C., Lambert J.-C. (2011) The GOME-2 total column ozone

791   product: Retrieval algorithm and ground-based validation, Journal of Geophysical Research,

792   vol. 116, D07302, Wiley-Blackwell

793   Marty, J., (2019). The IMS Infrasound Network: Current Status and Technolofical

794   Developments, in: Le Pichon, A., Blanc, E., Hauchecorn, A. (Eds.), Infrasound Monitoring

795   for Atmospheric Studies. Challenges in Middle Atmosphere Dynamics and Societal Benefits.

796   Springer Nature Switzerland AG, pp. 3–62. doi:10.1007/978-3-319-75140-5_1

797   McIntyre, M. E., & Palmer, T. N. (1983). Breaking planetary waves in the stratosphere.

798   Nature, 305(5935), 593-600.

799   Munro, R., Eisinger, M., Anderson, C., Callies, J., Corpaccioli, E., Lang, R., ... & Albinana,

800   A. P. (2006, June). GOME-2 on MetOp. In Proc. of The 2006 EUMETSAT Meteorological

801   Satellite Conference, Helsinki, Finland (Vol. 1216, p. 48).

802   Munro, R., et al. (2016): The GOME-2 instrument on the Metop series of satellites:

803   instrument design, calibration, and level 1 data processing – an overview, Atmos. Meas.

804   Tech., 9, 1279–1301, https://doi.org/10.5194/amt-9-1279-2016.

805   Peters, D., Hoffmann, P., & Alpers, M. (2003). On the appearance of inertia-gravity waves on

806   the north-easterly side of an anticyclone. Meteorologische Zeitschrift, 12(1), 25-35

807   Polvani, L. M., & Plumb, R. A. (1992). Rossby wave breaking, microbreaking, filamentation,

808   and secondary vortex formation: The dynamics of a perturbed vortex. Journal of Atmospheric

809   Sciences, 49(6), 462-476.

810   Pramitha, M., Venkat Ratnam, M., Taori, A., Krishna Murthy, B. V., Pallamraju, D., and

811   Vijaya Bhaskar Rao, S. (2015). Evidence for tropospheric wind shear excitation of high-

812   phase-speed gravity waves reaching the mesosphere using the ray-tracing technique, Atmos.

813   Chem. Phys., 15, 2709–2721, https://doi.org/10.5194/acp-15-2709-2015.

814   Rauthe, M., Gerding, M., Höffner, J., & Lübken, F. J. (2006). Lidar temperature

815   measurements of gravity waves over Kühlungsborn (54° N) from 1 to 105 km: A winter-

816   summer comparison. Journal of Geophysical Research: Atmospheres, 111(D24).

817

818   Wüst, S., & Bittner, M. (2006). Non-linear resonant wave–wave interaction (triad): Case

819   studies based on rocket data and first application to satellite data. Journal of atmospheric and

820   solar-terrestrial physics, 68(9), 959-976.

821

822   Wüst, S., Offenwanger, T., Schmidt, C., Bittner, M., Jacobi, C., Stober, G., Yee, J.H.,

823   Mlynczak, M. G. & Russell III, J. M. (2018). Derivation of gravity wave intrinsic parameters

824   and vertical wavelength using a single scanning OH (3-1) airglow spectrometer. Atmospheric

825   Measurement Techniques, 11(5), 2937-2947.

826
827   Smets, P.S.M., Evers, L.G. (2014). The life cycle of a sudden stratospheric warming from

828   infrasonic ambient noise observa-tions, J. Geophys. Res. Atmos., 119, 12,084-12,099

829   Spurr, R., Loyola, D., Heue, K. P., Van Roozendael, M., & Lerot, C. (2022). S5P/TROPOMI

830   Total Ozone ATBD. Deutsches Zentrum für Luft- und Raumfahrt (German Aerospace

831   Center), Weßling, Germany, Tech. Rep. S5P-L2-DLR-ATBD-400A.

832   Sutherland, L.C., Bass, H.E., (2004). Atmospheric absorption in the atmosphere up to 160

833   km. *J. Acoust. Soc. Am.,* 115, 1012–1032. https://doi.org/10.1121/1.1631937

834   Szuberla, C.A.L., Olson, J.V., (2004). Uncertainties associated with parameter estimation in

835   atmospheric infrasound rays. J. Acoust. Soc. Am. 115, 253-258. doi: 10.1121/1.1635407

836   Veefkind, J. P., Aben, I., McMullan, K., Förster, H., De Vries, J., Otter, G., ... & Levelt, P. F.

837   (2012). TROPOMI on the ESA Sentinel-5 Precursor: A GMES mission for global

838   observations of the atmospheric composition for climate, air quality and ozone layer

839   applications. Remote sensing of environment, 120, 70-83.

840

841